A multi-objective optimization-based layer-by-layer blade-coating approach for organic solar cells: rational control of vertical stratification for high performance

Rui Sun[1], Jie Guo[1], Qiang Wu[1], Zhuohan Zhang[2], Wenyan Yang[1], Jing Guo[1], Mumin Shi[1], Yaohong Zhang[3], Simon Kahmann[4], Long Ye[5], Xuechen Jiao[6], Maria A. Loi[4], Qing Shen[3], Harald Ade[5], Weihua Tang[2], Christoph J. Brabec[7], Jie Min[1]*

[1]The Institute for Advanced Studies, Wuhan University, Wuhan 430072, China
E-mail: min.jie@whu.edu.cn

[2]Key Laboratory of Soft Chemistry and Functional Materials, Ministry of Education, Nanjing University of Science and Technology, Nanjing 210094, China

[3]Faculty of Informatics and Engineering, The University of Electro-Communications, 1-5-1 Chofugaoka, Tokyo 182-8585, Japan

[4]Zernike Institute for Advanced Materials, University of Groningen, NL-9747AG Groningen, The Netherlands

[5]Department of Physics and Organic and Carbon Electronics Laboratory (ORaCEL), North Carolina State University, Raleigh, NC 27695, United States

[6]Department of Materials Science and Engineering, Monash University, Victoria, Australia.

[7]Institute of Materials for Electronics and Energy Technology (i-MEET), Department of Materials Science and Engineering, Friedrich-Alexander-Universität Erlangen-Nürnberg, Martensstr. 7, 91058 Erlangen, Germany

1. Experimental Section

1.1. Materials

Materials: J71 was purchased from Solarmer Materials Inc and used without further purification., ITC6-IC was provided by Weihua Tang's group. Solvents (chloroform and methanol) were dried and distilled from appropriate drying agents prior to use.

1.2. Blade-coating device fabrication and Testing

The solar cell devices were fabricated with a conventional structure of Glass/ITO/PEDOT: PSS(40 nm)/(donor: acceptor (D:A) for bulk heterojunction (BHJ) blend or D/A for layer-by-layer (LbL) blend, respectively) /PDINO/Al. Pre-patterned ITO coated glass substrates (purchased from South China Science &Technology Company Limited) washed with methylbenzene, deionized water, acetone, and isopropyl alcohol in an ultrasonic bath for 15 min each. After blow-drying by high-purity nitrogen, All ITO substrates are cleaned in ultraviolet ozone cleaning system for 15 minutes. Subsequently, a thin layer of PEDOT: PSS (Xi'an Polymer Light Technology Corp 4083) was deposited through spin-coating at 4,000 rpm for 30 s on pre-cleaned ITO-coated glass from a PEDOT: PSS aqueous solution and d annealed at 150 °C for 15 min in atmospheric air. Then the BHJ layer was blade-coating in ambient atmosphere from a solution of donor: acceptor (1:1, wt%; 15 mg mL^{-1}) in chloroform onto the PEDOT: PSS layer at a varied blade-coating speed for controlling the morphology and thickness of active layer. For the solar cells with a LbL architecture, donor material in chloroform solution (12 mg mL^{-1}) was bladed on PEDOT: PSS layer to form a front layer with pre-annealing, then a solution of acceptor (12 mg mL^{-1}) in chloroform was bladed onto the donor layer. After that, the active layers were annealed. Then methanol solution of PDINO at a concentration of 1.0 mgml^{-1} was spin-coated onto the active layer at 3000 rpm for 30s. To complete the fabrication of the devices, 100 nm of Al was thermally evaporated through a mask under a vacuum of ~5 × 10^{-6} mbar. The active area of the devices was 4 mm^2. For the flexible devices with a structure of polyethylene terephthalate (PET)/ITO-metal-ITO (IMI)/PEDOT: PSS/active layer/PDINO/Al, the processing methods are similar with the normal devices as mentioned above. In addition, for the stability measurements of relevant devices based on Ag as top electrode, 100 nm of Ag were also thermally evaporated through a mask under a vacuum of ~6 × 10^{-6} mbar. Here the active area of the devices was 10 mm^2. The devices were encapsulated by glass slides using epoxy in nitrogen filled glovebox prior to measurement in ambient condition. The current-voltage characteristics of the solar cells were measured under

AM 1.5G irradiation on an Enli Solar simulator (100 mW cm^{-2}). Before each test, the solar simulator was calibrated with a standard single-crystal Si solar cell (made by Enli Technology Co., Ltd., Taiwan, calibrated by The National Institute of Metrology (NIM) of China).

1.3 Instruments and Characterization

Photoluminescence measurements: *In-situ* PL measurements were conducted by QE65PRO spectrometer (Ocean Optics, USA) for investigating the film formation and thermal annealing treatments. In addition, the thermal degraded PL data and emission of relevant films were collected using a Zolix Flex One Spectrometer. The PL excitation wavelength was set to 532 nm.

Atomic force microscopy (AFM) measurements: AFM measurements were performed with a Nano Wizard 4 atomic force microscopy (JPK Inc. Germany) in Qi mode to observe the surface morphologies of the BHJ and LbL films deposited on glass substrates.

Transmission electron microscopy (TEM) measurements: TEM was performed on the FEI TITAN3 Themis 60-300 double aberration-corrected microscope at the Shenzhen Cauchy data Co. Ltd, equipped with the Super-X energy dispersive spectrometer.

Grazing incidence wide-angle X-ray scattering (GIWAXS) measurements: GIWAXS measurement was performed at the small and wide angle X-ray scattering beamline at the Australian Synchrotron. The 2-dimensional raw data were reduced and analyzed with a modified version of Nika. The GIWAXS patterns shown were corrected to represent real Q_z and Q_{xy} axes considering the missing wedge. The critical incident angle was determined using the maximized scattering intensity from sample scattering with negligible contribution from bottom layer scattering. The shallow incident angle scattering was collected at 0.02°, which rendered the incident X-ray an evanescent wave along the top surface of the thin films.

Time-of-flight secondary ion mass spectrometry (TOF-SIMS) measurements: TOF-SIMS experiments were conducted using a TOF-SIMS V (ION TOF, Inc. Chestnut Ridge, NY) instrument equipped with a Bi^{3+} liquid metal ion gun, Cesium sputtering gun, and electron flood gun for charge compensation. Cs^+ was used as the sputter source with a 10 keV energy and 6 nA current. The typical sputter area was 50 μm by 50 μm.

Optical measurements and simulations: Absorption spectra of the different store time blend solid thin films were measured on a Perkin Elmer Lambda 365 UV-Vis spectrophotometer. The optical simulations were calculated by Fluxim Setfos software.

Time-resolved PL (TRPL) spectroscopy measurements: Samples were kept under nitrogen atmosphere, mounted in an air-tight sample holder in a glovebox. Samples were excited at 400 nm using the second harmonic of a mode-locked Ti: sapphire laser (Mira 900, Coherent) delivering pulses of 150 fs width at a repetition rate of ≈76 MHz. The Ti: sapphire laser was pumped by a solid-state Nd: vanadate (Nd: YVO4) diode laser, frequency doubled, thus providing a single-frequency green (532 nm) output at 5 W. Steady-state spectra were recorded with an Imaging EM CCD camera (Hamamatsu). Time-resolved traces were taken with a Hamamatsu streak camera working in synchro-scan mode.

Femtosecond transient absorption spectroscopy (TAS) measurements: A femtosecond TA setup was used to study the photoexcited carrier dynamics. The laser source was a titanium/sapphire laser(CPA-2010, Clark-MXRInc.) with a wavelength of 775nm, arepa-tuition rate of 1kHz, and the pulse width is 150 fs. The light was separated into two parts. One part was incident on a sapphire plate to generate white light for the probe beam. The other part was used to pump an optical parametric amplifier(OPA) (aTOAPS from Quantronix) to generate light pulses to excite the sample. In this study, the pump light wavelength was 640 nm (1.94 eV), and the pump light intensity was 45μJ/cm^2. Time-resolved TA spectra were obtained from 530nm (2.34eV) to 750nm (1.65eV) with a temporal resolution of about 100fs. For all measurements, the pump and probe beams were incident on the glass side of the samples, and the TA measurements were carried out at room temperature.

Space charge limited current (SCLC) measurements: Single carrier devices were fabricated and the dark current-voltage characteristics measured and analyzed in the space charge limited (SCL) regime following the Ref.[1]. The structure of hole-only devices was Glass/ITO/PEDOT: PSS/Semiconductor layer/MoOx (10 nm)/Ag (100 nm). The reported mobility data are average values over the six devices of each sample.

Photo-induced charge carrier extraction by linearly increasing the voltage (photo-CELIV) measurements: In photo-CELIV measurements, the devices were illuminated with a 405 nm laser diode. Current transients were recorded across the internal 50 Ω resistor of our oscilloscope. Here, a fast electrical switch was used to isolate the device in order to prevent carrier extraction or sweep out. After the variable delay time, the switch connected the device

to a function generator. It applied a linear extraction ramp, which was 40 μs long and 2.0 V high. Moreover, it started with an offset matching the V_{oc} of the device for each delay time.

Transient photovoltage (TPV) measurements: For TPV measurements, devices were directly connected to an oscilloscope in open-circuit conditions (1MΩ). Then the device was illuminated with a white light LED at different light intensities. A small optical perturbation was applied using a 405 nm laser-diode which was adjusted in light intensity to produce a voltage perturbation of $\Delta Vo < 10\ mV \ll Voc$. The amount of charges generated by the pulse was obtained by integrating a photocurrent measurement (50 Ω) without bias light.

Charge extraction (CE) measurements: For CE measurements, it can be used to determine the charge density in the active layer of the device at any point in the *J-V* curve. The devices were held at a specified voltage in the dark or under illumination. At a certain time t_0 the light is switched off, the cell is switched to short-circuit conditions, and the resulting current transient is recorded with an oscilloscope. Most of the charge is extracted in a few microseconds due to a high internal electrical field at short circuit conditions. In addition, a fast analog switch from Texas Instruments (TS5A23159) is used to perform the switching from the specified voltage to short circuit conditions. It provides a very quick switching time (50 ns), a low on-state resistance (1 Ω), high off-state resistance (> 1MΩ) and a very low charge injection (<< 10^{15} $cm^2V^{-1}s^{-1}$). A Keithley 2440 source-measurement unit is used to set the initial device voltage.

Transient photocurrent (TPC) measurements: Relevant BHJ and LbL solar cells were excited with a 405 nm laser diode. The transient photocurrent response of the devices at short circuit condition to a 200 *μs* square pulse from the LED with no background illumination. The current traces were recorded on a Tektronix DPO3034 digital oscilloscope by measuring the voltage drop over a 5-ohm sensor resistor in series with the solar cell. DC voltage was applied to the solar cell with an MRF544 bipolar junction transistor in common collector amplifier configuration.

Fourier-transform photocurrent spectroscopy external quantum efficiency (FTPS-EQE) measurements: FTPS-EQE spectra were measured by using a Vertex 70 from Bruker optics and QTH lamp. The EL signature was collected with monochromator and detected with Si-CCD detector.

Stability measurements: Light-induced degradation testing: we performed light-induced degradation experiments with one sun equivalent illumination intensity for over 500 hours on

all three small molecules investigated in this study. The solar cells were fabricated in a glovebox and aged under high vacuum, excluding the well-known effects of oxygen degradation from our experiments. It is important to operate all devices at temperatures below their glass transition temperature (T_g) to avoid thermally induced morphological changes. We minimized the thermal degradation by using white light LED's. To exclude any other influence of the experimental conditions on the results, all the molecule systems were aged in the same test side by side. The investigated solar cells were built in a standard device architecture with PEDOT: PSS and PDINO/Al contacts. Note that the trends of two separated tests for these two blends are consistent. Thermal stability testing: The testing devices were fabricated under the same preparation conditions, as mentioned above. After the spin-coating of the active layer, the devices were transferred to a hot plate at 120 °C in a N_2-filled glovebox and annealed for various time periods. Then, the devices were quenched to room temperature before the cathode layers were thermally deposited. All the samples for time-dependent annealing measurements were prepared under the same conditions with the thermal stability testing ones. Blending stability testing: To insight the mechanical stability of the LbL and BHJ, we conducted the device structure of polyethylene terephthalate (PET)/ITO-metal-ITO (IMI)/PEDOT: PSS/active layer/PDINO/Al. We compared the blending stability of the two type blends fabricated devices under one sun illumination in dry nitrogen atmosphere with controlled O_2 and H_2O level below 0.1 ppm.
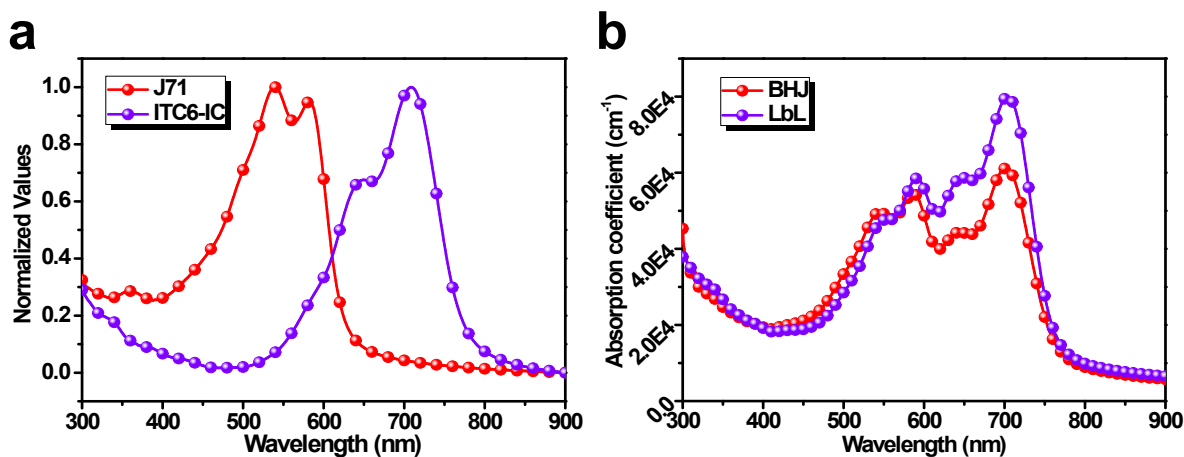
Fig. S1. (a) Normalized absorption spectra of pristine J71 and ITC6-IC blends; (b) Absorption coefficient of BHJ and LbL blends bladed.
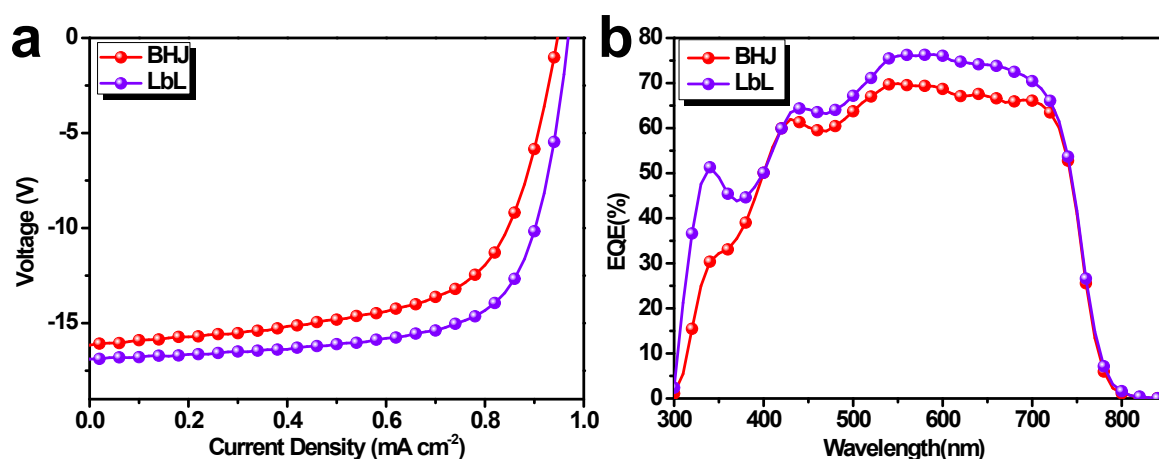

Fig. S2. (a) Current density-voltage (*J-V*) curves of the OSCs based on J71: ITC6-IC BHJ and J71/ITC6-IC LbL layers under the illumination of AM 1.5G at 100 mW cm^{-2}, (b) External quantum efficiency (EQE) curves of the relevant devices based on BHJ and LbL architectures.

Note that both optimal blends need to be treated by thermal annealing (TA) at 150 $^{\circ}$C for 5 minutes. The organic solar cells (OSCs) based on J71: ITC6-IC bulk heterojunction (BHJ) blend give the best performance with a power conversion efficiency (PCE) of 10.41%, with an open-circuit voltage (V_{oc}) of 0.950 V, a short-circuit current density (J_{sc}) of 16.15 mA cm^{-2}, and a fill factor (FF) of 67.79%. In addition, the optimized J71/ITC6-IC LbL device shows slightly higher V_{oc} (0.962 V), J_{sc} (16.85 mA cm^{-2}) and FF (70.10%) values as compared to its BHJ counterpart, and thus results in an increased PCE of 11.47%. As exhibited in **Fig. S2b**, layer by layer (LbL) device shows the higher response in the External quantum efficiency (EQE) curve, implying the efficient photoelectron conversion. The calculated J_{sc} values integrated from the EQE curves match well with those obtained from the current density-voltage (*J-V*) measurements within 3% mismatch.

Table S1. Photovoltaic parameters of the OSCs based on J71: ITC6-IC BHJ and J71/ITC6-IC LbL layers under the illumination of AM 1.5G at 100 mW cm^{-2}, and photoluminescence quenching (PLQ) efficiency from the corresponding blend films.

Active layers	V_{oc} (V)	J_{sc} (mA cm^{-2})	FF (%)	PCE[a] (%)	PLQ (%)
BHJ	0.950	16.15	67.79	10.41 [10.06]	90%
LbL	0.968	16.85	70.10	11.47 [11.18]	93%

[a]The values in square bracket are the average PCE obtained from ten devices.
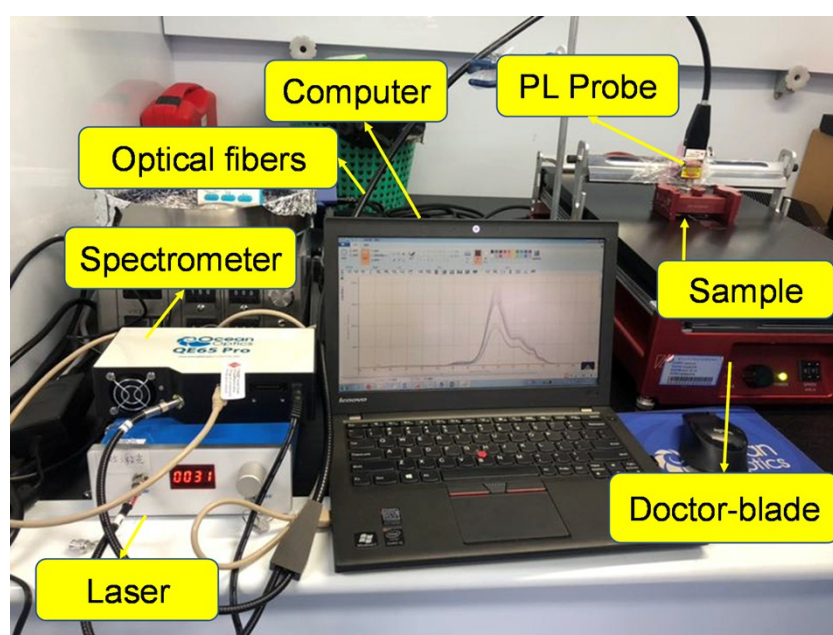
Fig. S3. Photo of the *in-situ* photoluminescence (PL) setup as well as its simple schematic representation.
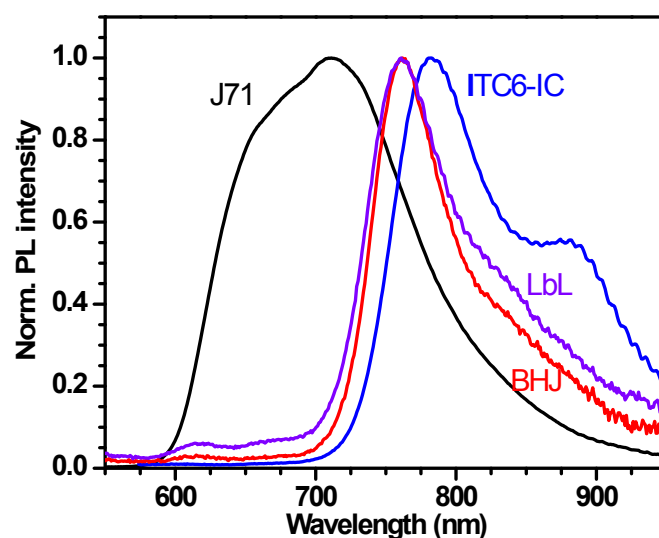
Fig. S4. Normalized photoluminescence (PL) spectra of pristine J71 and ITC6-IC films and their blends based on BHJ and LbL structures.
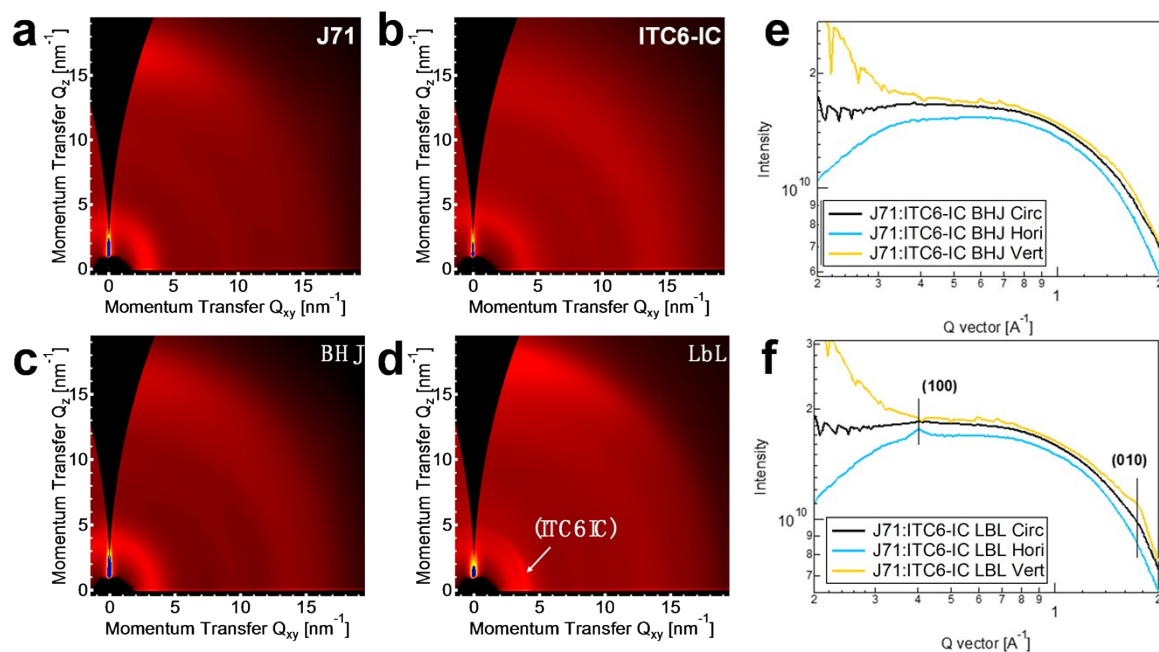
Fig. S5. 2D GIWAXS patterns of (a) pristine J71 film, (b) pristine ITC6-IC film acquired at the critical incident angle of 0.13°. 2D GIWAXS patterns of (c) BHJ film and (d) LbL film acquired at the critical angle of 0.02°. In addition, 1D GIWAXS profiles of (e) J71: ITC6-IC BHJ film, (f) J71/ITC6-IC LbL film acquired at the critical angle of 0.02°.
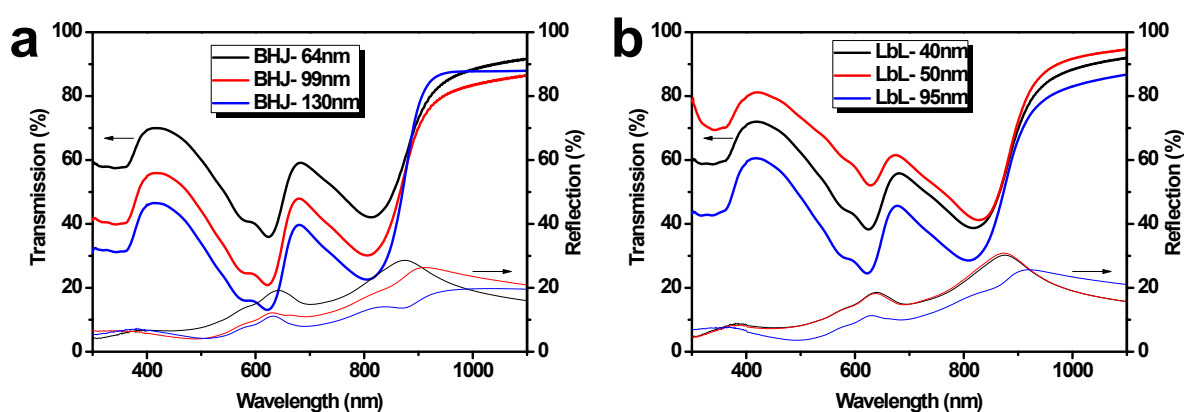
**Fig. S6**. Transmission and reflection spectra of BHJ and LbL blends with different thicknesses.
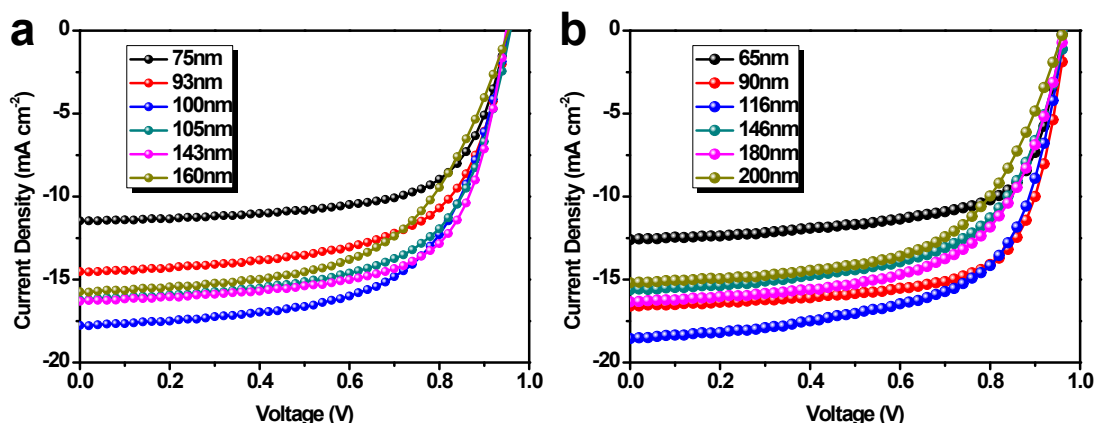
Fig. S7. *J-V* curve characteristics of BHJ and LbL devices based on different thicknesses.

Table S2. Photovoltaic parameters of the OSCs based on J71: ITC6-IC BHJ and J71/ITC6-IC LbL layers with different thicknesses, measured under one sun.

Blends	Speed	Thickness [nm]	Voc [V]	Jsc [mA cm^{-2}]	FF [%]	PCE(PCE[a]) [%]
BHJ	18	75	0.952	11.46	66.42	7.24(7.16)
	20	93	0.955	14.53	62.94	8.87(8.56)
	22	100	0.954	17.75	61.42	10.40(10.34)
	25	105	0.957	16.24	62.83	9.76(9.52)
	30	143	0.961	16.31	60.10	9.42(9.30)
	40	160	0.954	15.73	57.78	8.67(8.50)
LbL	15	65	0.961	12.60	67.36	8.16(8.08)
	18	90	0.968	16.89	70.10	11.46(11.22)
	20	116	0.966	18.57	63.47	11.38(11.25)
	25	146	0.969	17.20	61.31	10.21(10.08)
	30	180	0.965	16.33	61.86	9.75(9.54)
	40	200	0.963	16.29	59.47	9.32(9.18)

a) The values in square bracket are the average PCE obtained from five devices.
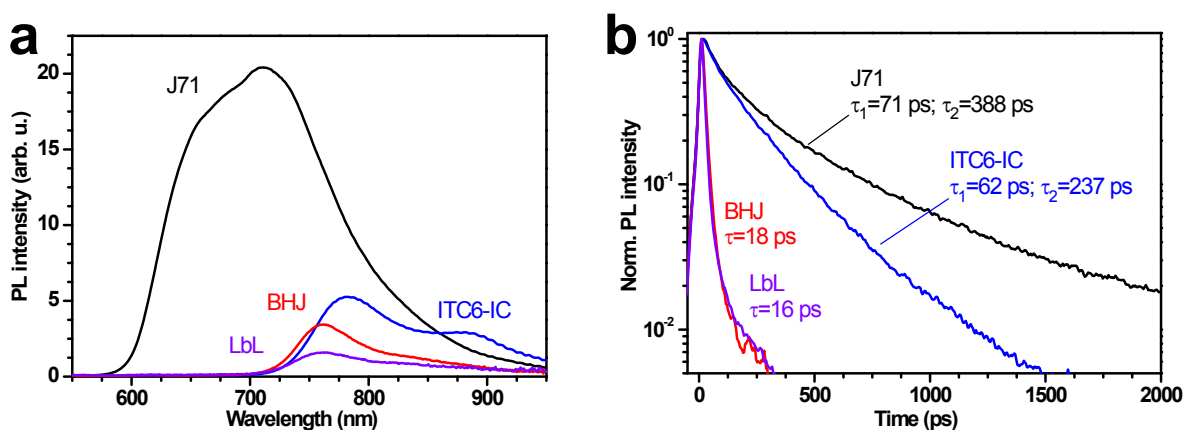
Fig. S8. (a) Photoluminescence (PL) spectra of pristine J71 and ITC6-IC films and their blends based on BHJ and LbL structures. (b) Corresponding normalized decays of the PL intensity of neat films and those of blend films taken at maximum emission. All films were excited at 400 nm.
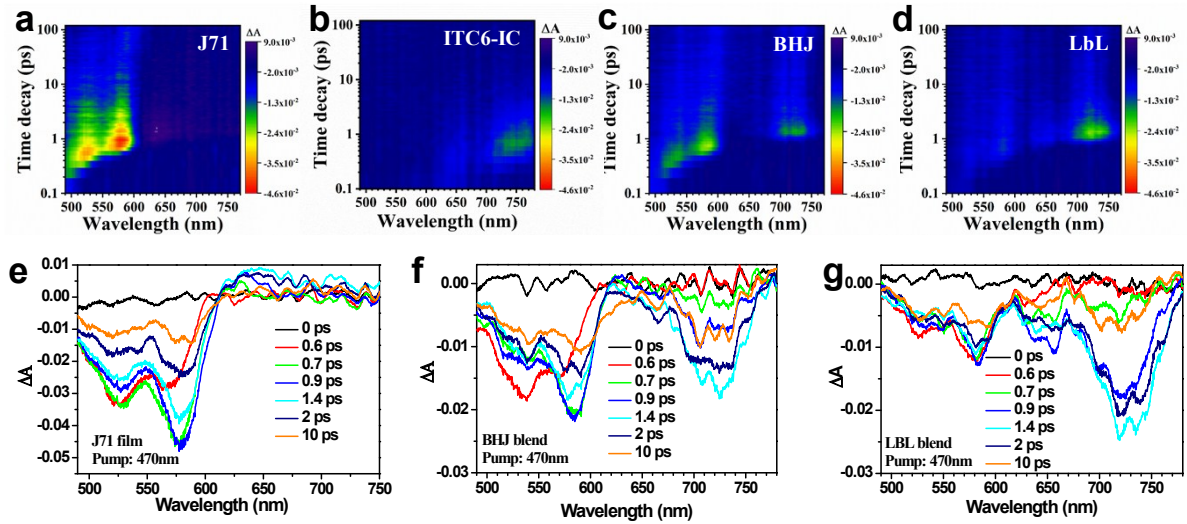
Fig. S9. fs-ns transient spectra of the pristine (a) J71 and (b) ITC6-IC films as well as their (c) BHJ and (d) LbL blends excited at 470 nm. Transient absorption spectra for (e) pristine J71 film, (f) BHJ blend and (c) LbL blend.

Table S3. Summary of the dynamics for pure J71 and ITC6-IC films.

Films	Wavelength	A_1	$\tau_{1(ps)}$	A_2	$\tau_{2(ps)}$	A_3
J71	592	-0.45 ± 0.03	8.1 ± 1.4	-	129 ± 18	-
ITC6-	730	-0.32 ± 0.03	$11.7 \pm 2.$	-	136 ± 43	-

**Table S4**. Summary of the calculated results of the hole injection time and rate in BHJ and LbL films.

Films	$\tau_{inj(ps)}$	$k_{inj(s^-}$	$\eta_{inj(\%)}$
BHJ	0.45 ± 0.06	2.2	89.7%
LbL	1.05 ± 0.04	0.95	95.3%

Hole injection efficiency: The hole injection (or collection) efficiency (η_{inj}) was calculated according to Equation S1 and S2, where $\tau_{1}\text{-}A$ is the average lifetime of singlet excitons in pristine ITC6-IC films, k_{rec} is the recombination rate in pristine ITC6-IC films. and k_{inj} is the

hole injection rate in blended films. Both lifetimes were obtained from transient absorption measurements. Here the $\tau_{1\text{-}A}$ and k_{rec} values of pristine ITC6-IC films are 1.8 ± 0.1 ps and 0.56 ps^{-1}, respectively.

$$\eta_{inj} = \frac{k_{inj}}{(k_{inj} + k_{rec})}$$ Equation S1

$$k_q = \frac{1}{k_{inj} + 1/\tau_{1\text{-}A}}$$ Equation S2
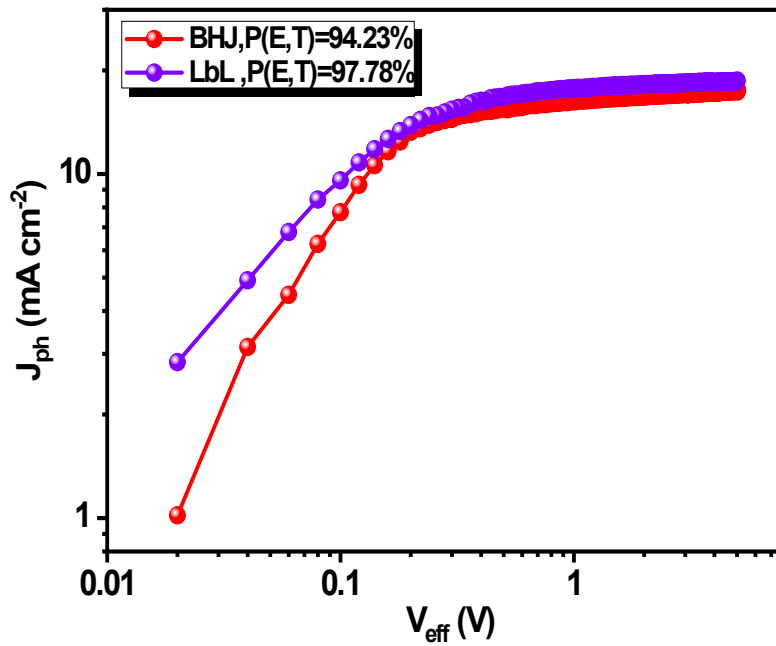
Fig. S10. Photocurrent density (J_{ph}) plotted against the internal voltage (V_{in}) for the devices processed with BHJ and LbL approaches, respectively. The measured photocurrent is given by $J_{ph} = J_L - J_D$, where JL is the current density under illumination and JD, is the current density in dark condition. The V_{in} is defined by $V_{in} = V_o - V$, where V_o is the voltage at which J_{ph} is zero and V is the applied bias voltage.[2] Thus, V_{in} corresponds to the strength of electric field within the device to extract the charge carriers. In the high regime ($V_{in} > 3V$), almost all of the photogenerated free charges within the device can be collected, and the J_{ph} represents the efficiency of charge generation in that device. The increased J_{ph} of LbL device at higher V_{in} can be attributed to a high photoabsorption rate in the device and a decrease in extraction limited recombination due to a higher internal electric field.
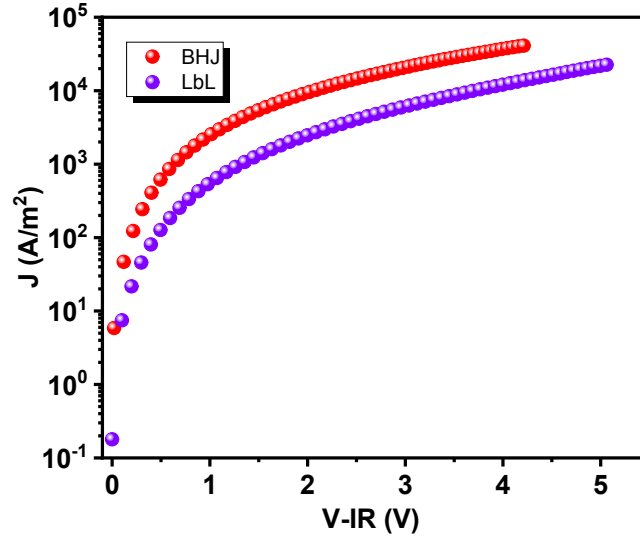
Fig. S11. The dark *J-V* characteristics of BHJ and LbL hole-only devices. The solid lines represent the best fitting using the SCLC modified Mott-Gurney model. The *J-V* characteristics of hole-only diodes with a structure of ITO/ PEDOT: PSS/BHJ or LbL/MoO3/Ag can be excellently fit to the Mott-Gurney relation for space charge limited current:[3]

$$J_{SCL} = \frac{9}{8}\varepsilon_0\varepsilon_r\mu\frac{V_{in}^2}{L^3}exp\left(\frac{0.89 \times \beta}{\sqrt{L}}\sqrt{V_{in}}\right)$$, where J_{SCL} is the current density, ε_0 is the permittivity of free-space, ε_r is the relative dielectric constant of the active layer, μ is the charge carrier mobility, β is the field activation factor, L is the thickness of the device and V_{in} is the voltage dropped across the sample.
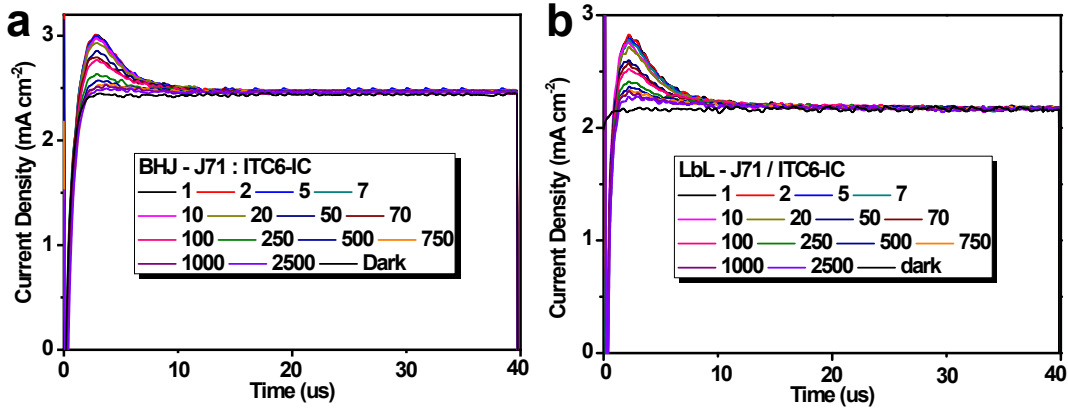
Fig. S12. Photo-CELIV measurements on the optimized BHJ (a) and LbL (b) devices for different delay times between the light pulse and the extraction voltage ramp.

Here we further employed the photo-CELIV technique to analyze charge carrier transport, charge carrier lifetime ($\tau_{\Delta n}$) and density (*n*), as well as relevant recombination kinetics in these two systems. The photo-CELIV technique is utilized to not only simultaneously determine the charge carrier lifetime and density, but also to gain a deeper understanding of the charge carrier transport and recombination dynamics in the device. When a reverse triangular-shaped bias is applied with an increasing rate *A* (V s⁻¹) in the dark to low conductivity materials such as

polymer solar cells, a rectangular-shaped current transient having a constant value is measured as an electrical signal. The constant current value of this transient stands for the capacitive displacement current $j(0)$ (C s^{-1}) of the sample. When the device is exposed to pulsed laser excitation, charge carriers are generated in the photoactive layer, and they either recombine or are extracted by the electric field. By measuring the maximum charge extraction current, t_{max}, which occurs at the maximum photocurrent and comparing the ratio of extracted current (Δj) to constant current ($j(0)$), we can calculate the charge carrier mobility using Equation S3.[2]

$$\mu = \frac{2d^2}{3At_{max}^2[1 + 0.36\frac{\Delta j}{j(0)}]} \quad if\ \Delta j \leq j(0)$$

Equation S3

Where d is the thickness of the active layer, A is the voltage rise speed A = dU/dt, U is the applied voltage to the device. In this measurement, the applied maximum voltage is 2V, with active layer thickness around 100 nm, the maximum electric field is thus $\sim 2 \times 10^5$ Vcm^{-1}. The Photo-CELIV transients recorded at room temperature at various delay times between the light pulse and the extraction pulse with these two systems are shown in Figure S11.

Table S5. Parameters extracted from Photo-CELIV signals within these two systems.

Blends	μ [cm^{2}V^{-1}s^{-1}]	$n0$ (cm^{-3})	τ_B [s]	t_{tr} [s]	β_L[cm^{3}s^{-1}]	l_d[nm]
BHJ	8.41×10^{-5}	3.50×10^{15}	5.59×10^{-5}	2.38×10^{-7}	5.63×10^{-11}	379
LbL	1.62×10^{-4}	1.86×10^{15}	1.31×10^{-4}	1.23×10^{-7}	1.09×10^{-10}	466
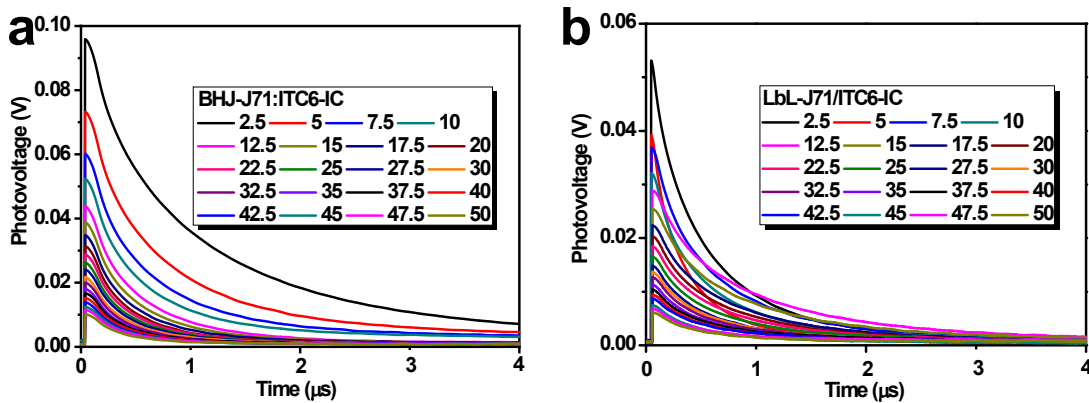
Fig. S13. TPV measurements on the optimized BHJ (a) and LbL (b) devices for light intensities of 0.15 to 2.50 sun. Transient photovoltage (TPV) measurements were used to analyze the recombination of free charges within the working devices by recording the transient voltage decay of the device under open circuit conditions under continuous illumination before a small perturbative light pulse was injected.
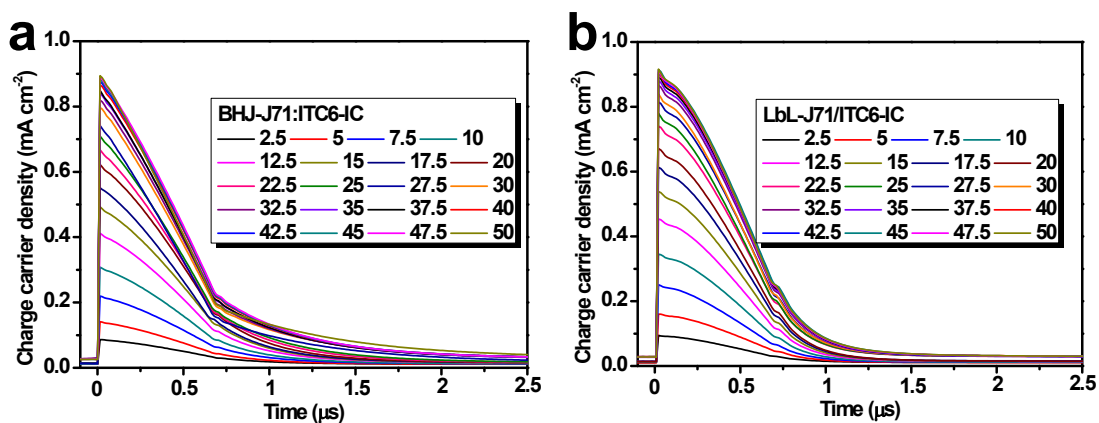
Fig. S14. TPV measurements on the optimized BHJ (a) and LbL (b) devices for light intensities of 0.15 to 2.50 sun.
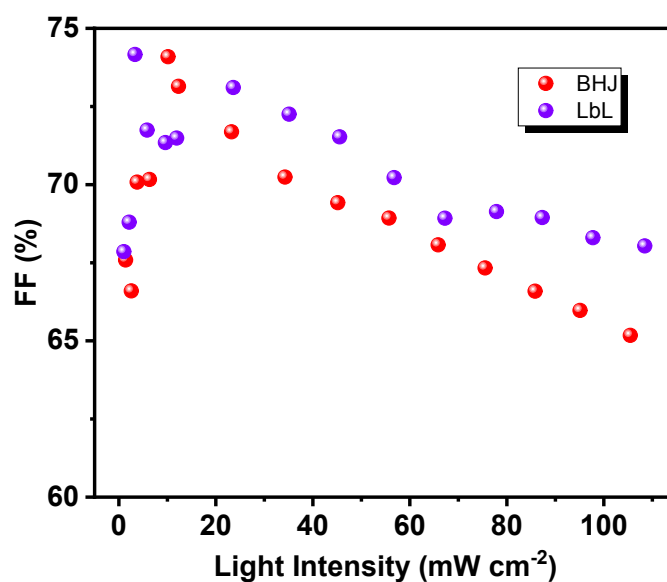
Fig. S15. The measured FF of BHJ and LbL devices as a function of illumination intensity (symbols).

To further gain insight into the influence of blend morphology and charge transport caused by the various blend morphologies on the device performance, we studied the light intensity dependence of *J-V* characteristics, which has been demonstrated to be a powerful tool for probing the dominant recombination mechanisms. The *J-V* characteristics of the BHJ and LbL devices under the illumination intensities ranging from 105 to 1.5 mW cm^{-2}. The light intensity dependence of the FF for each system are presented in **Fig. S14**. The FF (over 65%) remains relatively constant within the light intensity range from 100 to 10 mW cm^{-2} for the LbL device, indicating that the active layer is sufficiently good to ensure efficient charge extraction. The FF

of the BHJ device, in contrast, shows a larger variation with light intensity, indicating that the recombination losses become dominant at higher current densities.
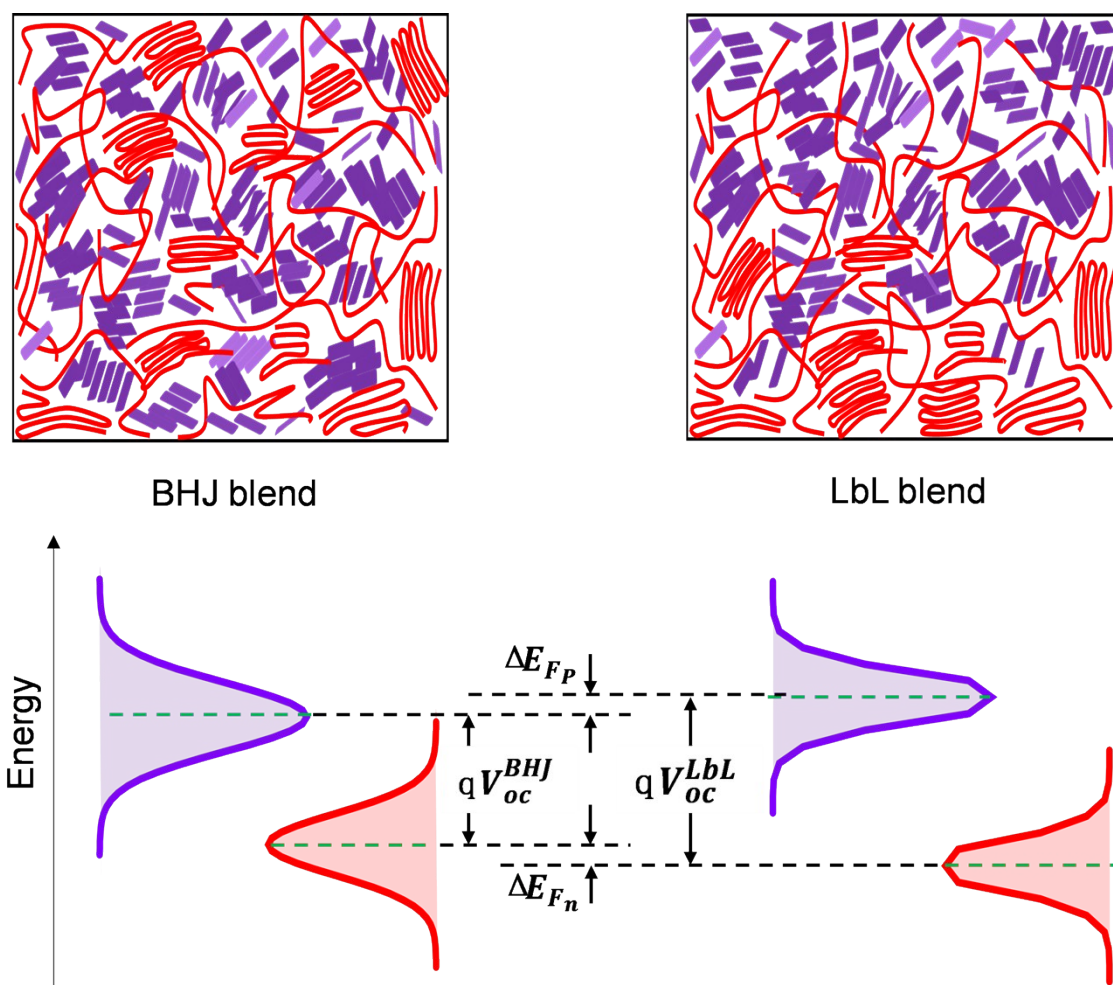
Fig. S16. Top: structure model of BHJ and LbL blends (blue line: J71; red dot: ITC6-IC). Bottom: Energy scheme showing the DOS in both BHJ and LbL devices. Additionally, unlike the BHJ blend, the donor material is enriched in the bottom of LbL blend, and the acceptor material is enriched in the upper layer. Thus, the corresponding electron quasi-Fermi level (E_{Fn}) of acceptor can be up-shifted and the hole quasi-Fermi level (E_{Fp}) will be down-shifted in the LbL layer.
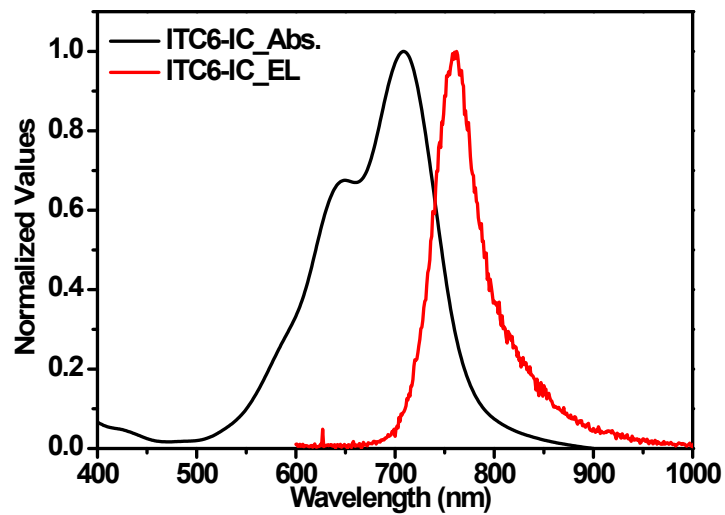
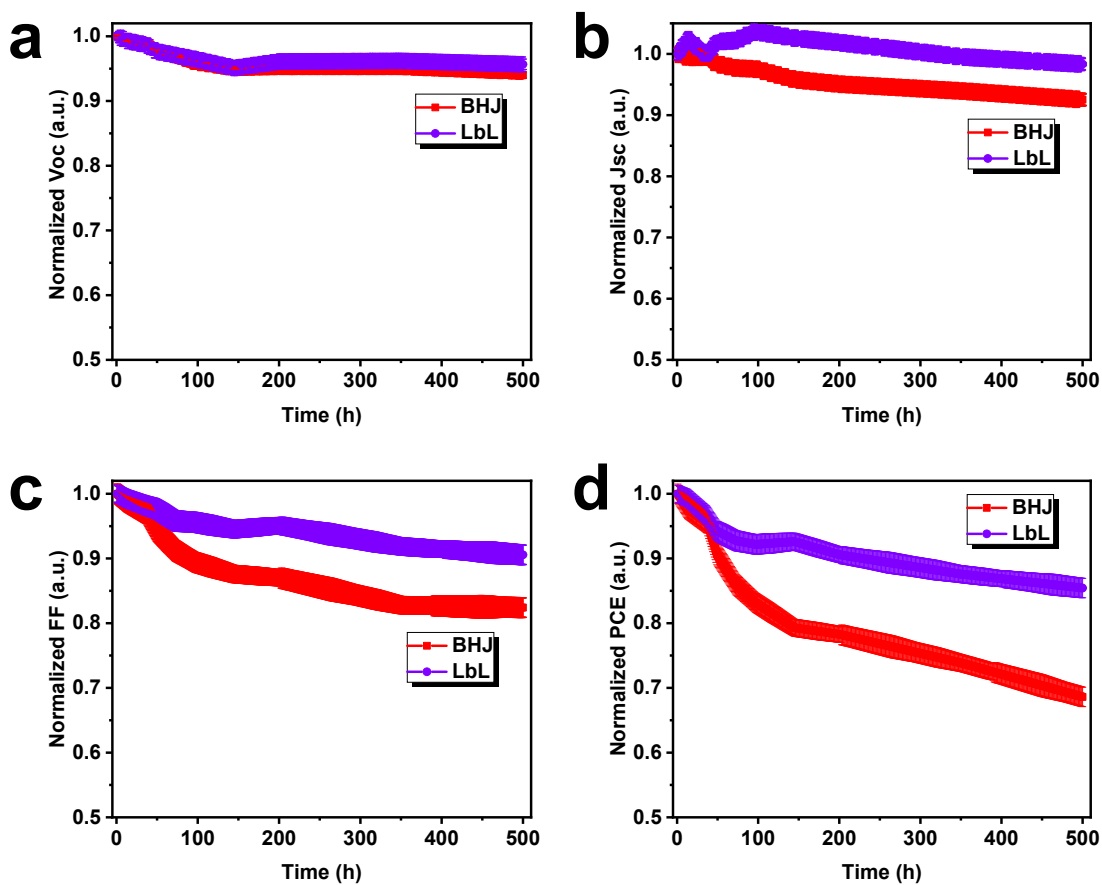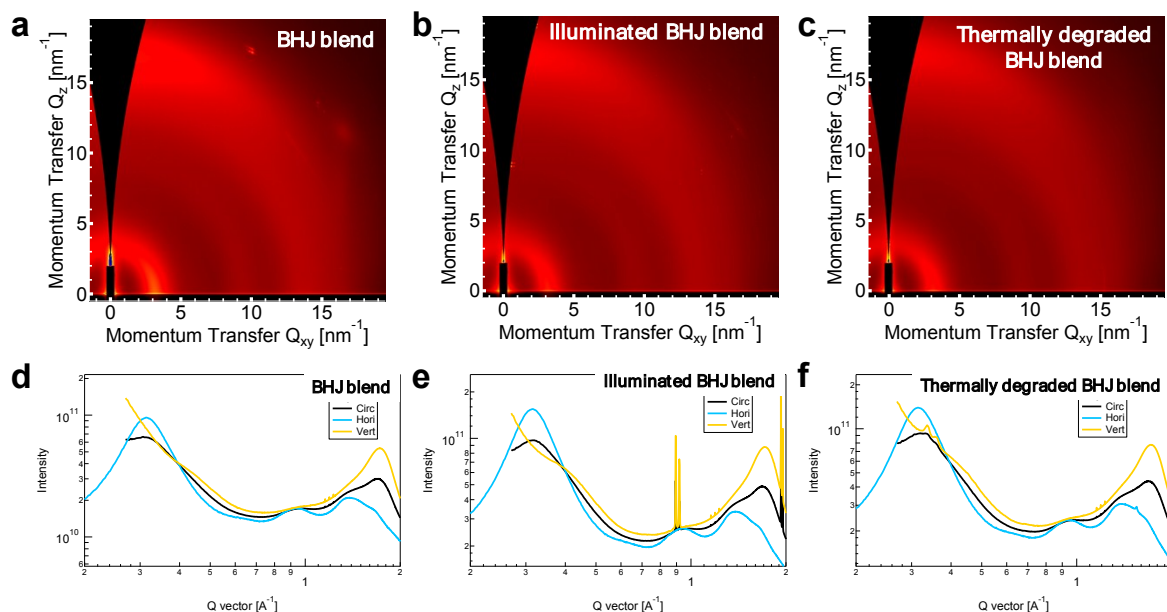**Fig. S17**. The emission and absorption spectra of ITC6-IC.

Fig. S18. Normalized V_{oc}, J_{sc}, FF and PCE values of BHJ and LbL devices illuminated under one sun over 500 hours.

Fig. S19. 2D GIWAXS patterns of (a) optimal BHJ film, (b) BHJ blend under illumination over 500 hours and (c) BHJ blend annealed at 120 °C over 1500 h; (d) GIWAXS profiles of (a) image; (e) GIWAXS profiles of (e) image; (f) GIWAXS profiles of (c) image. All films were acquired at the critical angle of 0.13°.
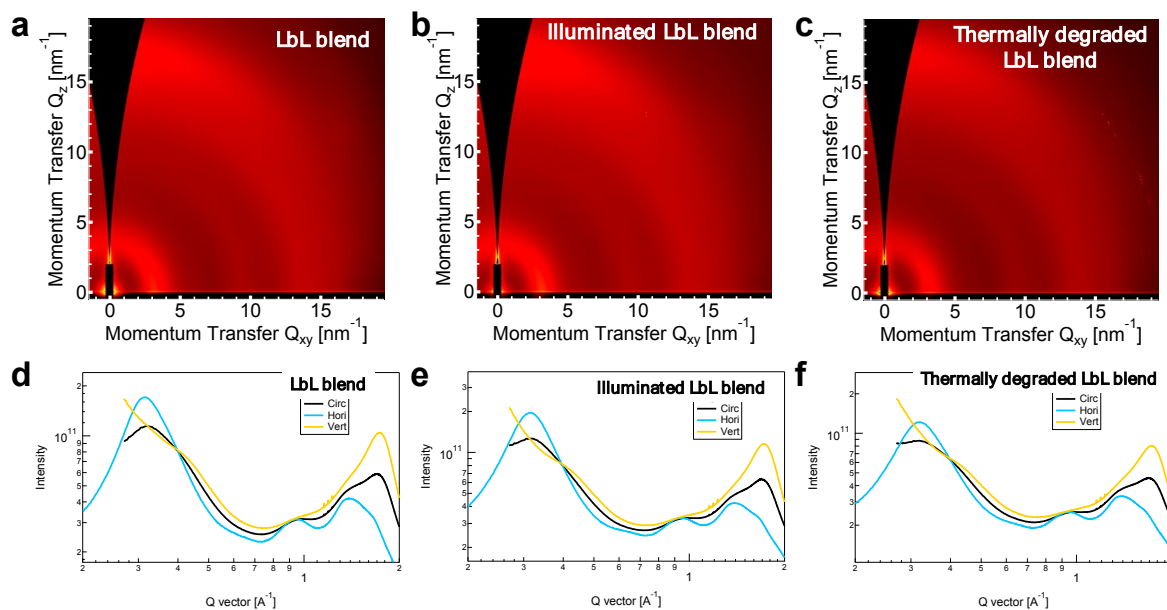
Fig. S20. 2D GIWAXS patterns of (a) optimal LbL film, (b) LbL blend under illumination over 500 hours and (c) LbL blend annealed at 120 °C over 1500 h; (d) GIWAXS profiles of (a) image; (e) GIWAXS profiles of (e) image; (f) GIWAXS profiles of (c) image. All films were acquired at the critical angle of 0.13°.

References

1.   R. Sun, J. Guo, C. Sun, T. Wang, Z. Luo, Z. Zhang, X. Jiao, W. Tang, C. Yang, Y. Li, J. Min, *Energy Environ Sci*, **2019**, *12*, 384-395.

2.   J. Min, Y. N. Luponosov, N. Gasparini, M. Richter, A. V. Bakirov, M. A. Shcherbina, S. N. Chvalun, L. Grodd, S. Grigorian, T. Ameri, S. A. Ponomarenko, C. J. Brabec, *Adv Energy Mater*, **2015**, *5*, 1500386.
3.   T. Wang, R. Sun, S. Xu, J. Guo, W. Wang, J. Guo, X. Jiao, J. Wang, S. Jia, X. Zhu, Y. Li, J. Min, *J. Mater. Chem. A*, **2019**, *7*, 14070-14078.